Jensen et al., http://www.jgp.org/cgi/content/full/jgp.201210820/DC1

Simulation and analysis details

Simulations were performed on a special-purpose machine, Anton, designed for MD simulations (Shaw et al., 2009) in the *NPT* ensemble (310 K, 1 bar, Berendsen coupling scheme with one temperature group; Berendsen et al., 1984). All bond lengths to hydrogen atoms were constrained using M-SHAKE (Kräutler et al., 2001). Van der Waals and short-range electrostatic interactions were cut off at 10 Å. Long-range electrostatic interactions were calculated using GSE (Shan et. al., 2005) with a 64 × 64 × 64 FFT mesh. The simulation time step was 2 fs (2.5 fs in simulations 14 and 15); long-range electrostatics were evaluated every third step. The protein was initially relaxed in the membrane before a constant electric field was applied (Table S1). The field was increased linearly to full strength over a time period of <1 µs and held constant thereafter. Trajectories were saved at 300-ps intervals and analyzed using HiMach (Tu et al., 2008), which integrates visual MD (VMD) and its plugins (Humphrey et al., 1996). The electrostatic GSE potential (Φ_{GSE}) was computed on a three-dimensional grid with 0.8-Å resolution with a HiMach implementation of VMD's PMEPOT plugin.

REFERENCES

Allen, T.W., O.S. Andersen, and B. Roux. 2003. Structure of gramicidin A in a lipid bilayer environment determined using molecular dynamics simulations and solid-state NMR data. *J. Am. Chem. Soc.* 125:9868–9877. http://dx.doi.org/10.1021/ja029317k

Berendsen, H.J.C., J.P.M. Postma, W.F. van Gunsteren, A. Di Nola, and J.R. Haak. 1984. Molecular dynamics with coupling to an external bath. *J. Chem. Phys.* 81:3684–3690. http://dx.doi.org/10.1063/1.448118

Humphrey, W., A. Dalke, and K. Schulten. 1996. VMD: visual molecular dynamics. *J. Mol. Graph.* 14:33–38. http://dx.doi.org/10.1016/0263-7855(96)00018-5

Jensen, M.Ø., D.W. Borhani, K. Lindorff-Larsen, P. Maragakis, V. Jogini, M.P. Eastwood, R.O. Dror, and D.E. Shaw. 2010. Principles of conduction and hydrophobic gating in K^+ channels. *Proc. Natl. Acad. Sci. USA.* 107:5833–5838. http://dx.doi.org/10.1073/pnas.0911691107

Klauda, J.B., R.M. Venable, J.A. Freites, J.W. O'Connor, D.J. Tobias, C. Mondragon-Ramirez, I. Vorobyov, A.D. MacKerell Jr., and R.W. Pastor. 2010. Update of the CHARMM all-atom additive force field for lipids: validation on six lipid types. *J. Phys. Chem. B.* 114:7830–7843. http://dx.doi.org/10.1021/jp101759q

Koeppe, R.E., 2nd, J.A. Killian, and D.V. Greathouse. 1994. Orientations of the tryptophan 9 and 11 side chains of the gramicidin channel based on deuterium nuclear magnetic resonance spectroscopy. *Biophys. J.* 66:14–24.

Kräutler, V., W.F. van Gunsteren, and P.H. Hünenberger. 2001. A fast SHAKE algorithm to solve distance constraint equations for small molecules in molecular dynamics simulations. *J. Comput. Chem.* 22:501–508. http://dx.doi.org/10.1002/1096-987X(20010415)22:5<501::AID-JCC1021>3.0.CO;2-V

MacKerell, A.D., Jr., D. Bashford, M. Bellott, R.L. Dunbrack Jr., J.D. Evanseck, M.J. Field, S. Fischer, J. Gao, H. Guo, S. Ha, et al. 1998. All-atom empirical potential for molecular modeling and dynamics studies of proteins. *J. Phys. Chem. B.* 102:3586–3616. http://dx.doi.org/10.1021/jp973084f

Shan, Y., J.L. Klepeis, M.P. Eastwood, R.O. Dror, and D.E. Shaw. 2005. Gaussian split Ewald: A fast Ewald mesh method for molecular simulation. *J. Chem. Phys.* 122:054101. http://dx.doi.org/10.1063/1.1839571

Shaw, D.E., R.O. Dror, J.K. Salmon, J.P. Grossman, K.M. Mackenzie, J.A. Bank, C. Young, M.M. Deneroff, B. Batson, K.J. Bowers, et al. 2009. Millisecond-scale molecular dynamics simulations on Anton. SC '09 Proceedings of the Conference on High Performance Computing, Networking, Storage and Analysis. Association for Computing Machinery, New York, NY. 1–11. http://dx.doi.org/10.1145/1654059.1654099

Townsley, L.E., W.A. Tucker, S. Sham, and J.F. Hinton. 2001. Structures of gramicidins A, B, and C incorporated into sodium dodecyl sulfate micelles. *Biochemistry.* 40:11676–11686. http://dx.doi.org/10.1021/bi010942w

Tu, T., C.A. Rendleman, D.W. Borhani, R.O. Dror, J. Gullingsrud, M.Ø. Jensen, J.L. Klepeis, P. Maragakis, P. Miller, K.A. Stafford, and D.E. Shaw. 2008. A scalable parallel framework for analyzing terascale molecular dynamics simulation trajectories. SC '08 Proceedings of the 2008 ACM/IEEE conference on Supercomputing. IEEE Press, Piscataway, NJ.

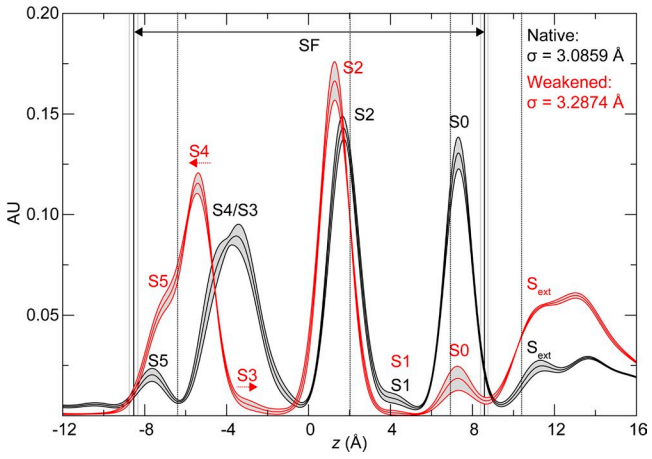

Figure S1. Thermodynamic K^+ distribution in $K_V1.2$ obtained with native and weakened LJ ion–SF interaction strength. Upper and lower curves correspond to one standard error of the mean, reflecting the variation of these distributions with the magnitude of applied voltage. Vertical dashed lines delineate the K^+-binding site grouping used for single-ion kinetics analysis in Fig. 2 E of the main text. At weakened interaction strength, the SF bound K^+ less tightly and the ion density shifted: the density in the coalesced site S4/S3 separated into two separate sites, S4 and S3 (indicated by red arrows), and the external binding site, S_{ext}, became relatively more populated, whereas the population of S0 decreased.

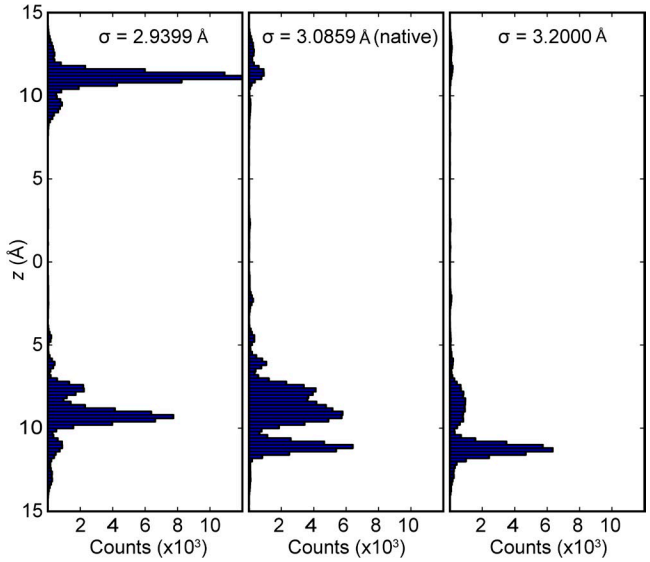

Figure S2. K^+ distribution in gA obtained with varying LJ ion–pore interaction strength. Smallest σ (in Å; strongest interaction strength) led to an increased propensity of K^+ to be in the vestibules ($z \approx \pm 10$ Å), native σ increased the propensity of K^+ to move from vestibule to lumen, and largest σ (weakest interaction strength) lowered K^+ recruitment from the surrounding solution to the pore vestibule.

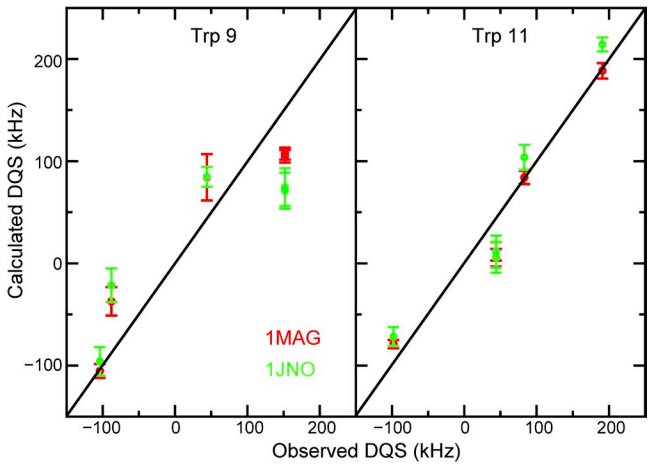

Figure S3. gA deuterium quadrupole splittings (DQS) of tryptophan (Trp) residues 9 and 11 obtained from simulations of 1MAG and 1JNO. Experimental values are from Koeppe et al. (1994). Each residue has five deuterium-labeled sites. Allen et al. (2003) found from 10 10-ns simulations initiated in the 1MAG structure an average DQS RMSD for Trp 9 of 74.6 kHz relative to the experimental value, whereas simulations initiated from 1JNO had a smaller RMSD of 23.2 kHz (Trp11, Trp13, and Trp15 were found to have RMSDs of 18.9 kHz in the 1JNO structure). In our 200-ns simulations (with an ion in the intracellular vestibule), however, the results did not depend substantially on the starting structure, and the DQS RMSDs for 1MAG were reduced to 40 and 23 kHz for Trp 9 and Trp 11, respectively. This is consistent with the finding that both structures relax to the same distribution of rotameric states (Fig. S4).

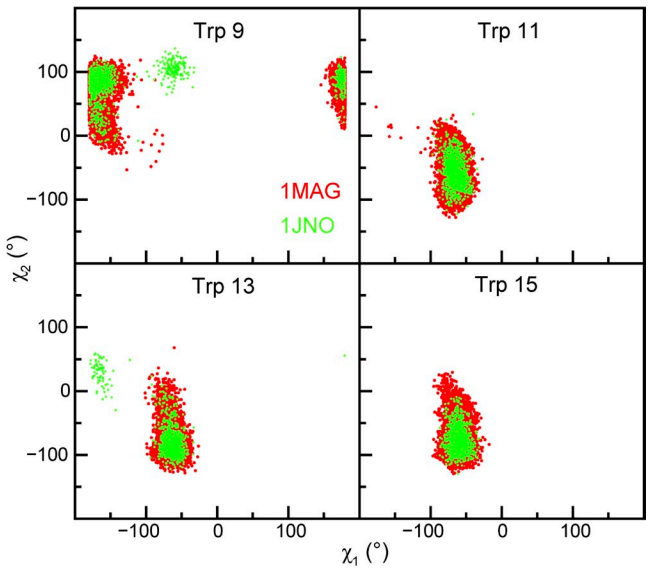

Figure S4. Tryptophan rotameric states in simulations starting from 1MAG and 1JNO. Allen et al. (2003) suggested that the most populated Trp 9 side-chain rotamer should be −170°, 90° (χ_1, χ_2), whereas the other Trp residues should assume −70°, −90°. Although in the 1MAG crystal structure the rotameric states differ from these values, after simulation the rotameric states obtained in our simulations of both 1JNO and 1MAG do agree with the suggested values, and both structures appear to have relaxed to a conformation exhibiting the same distribution of these rotameric states.

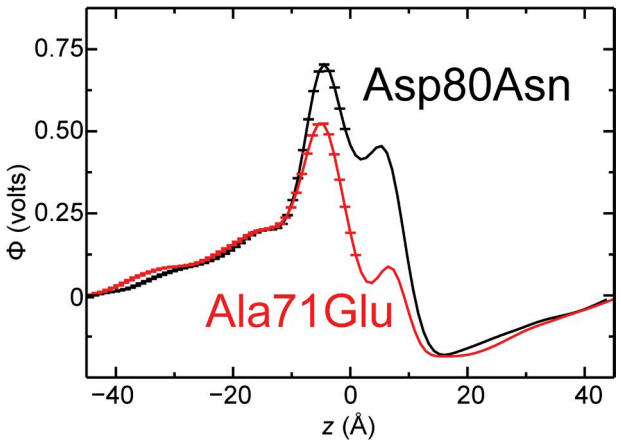

Figure S5. KcsA electrostatic profiles. Mutation of Asp80 to an asparagine residue (i.e., removal of negative charge) increased the potential at the center, whereas reintroduction of a wild-type glutamate residue at position 71 instead of alanine lowered the potential. These two profiles were obtained in the presence of an applied electric field, as reflected by the almost constant slope of the potential at $|z| > 20$ Å, while including only simulation snapshots where three ions were bound inside the SF and no ions were present in the cavity.

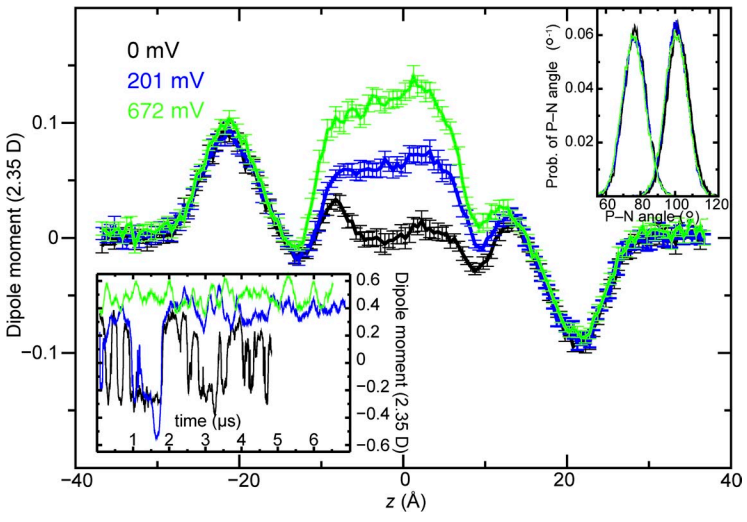

Figure S6. Water and lipid head-group orientation in gA. The water dipole moment (z component only) was calculated from simulations with no ions in the system and at different applied voltages (simulations 17–19); θ is the angle between the (unit) water dipole vector and the z axis. (Inset; bottom left) The z component of the pore–water dipole moment per molecule (in units of 2.35 D) is graphed as a function of time. (Inset; top right) The distribution of the lipid head group P–N vector tilt angle is graphed relative to the z axis. The lipid head-group orientation was found to be independent of the applied voltage used in the simulation. The orientation of the single-file water molecules inside the pore ($|z| < 20$ Å) differed with voltage. At 0 mV, the water molecules aligned with their dipoles either parallel or antiparallel to the z axis, and P_1 on average equaled zero; they reoriented (concertedly) with a rate of $\sim 3.6\ \mu s^{-1}$. With the field applied along $+z$, the propensity of water molecules to align with their dipoles parallel to the field increased; P_1 was thus greater than zero and increased with the magnitude of the applied field. The reduced net water orientation inside the pore at lower voltages increased the pore electrostatic potential (Fig. 4 G), opposing ion permeation.

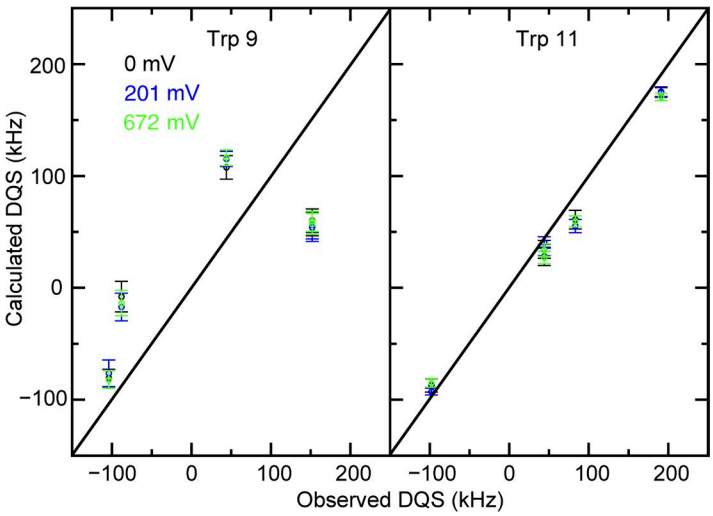

Figure S7. gA (1MAG) deuterium quadrupole splittings (DQS) of tryptophan (Trp) residues 9 and 11 at different applied voltages. The data indicate that the average orientation of these two Trp residues is independent of the applied field. Consequently, voltage-dependent conformational changes of these two residues appear not to influence ion permeation; their contribution to the pore electrostatic potential in Fig. 4 G in the main text is similar at all voltages. See the Fig. S3 legend for more details.

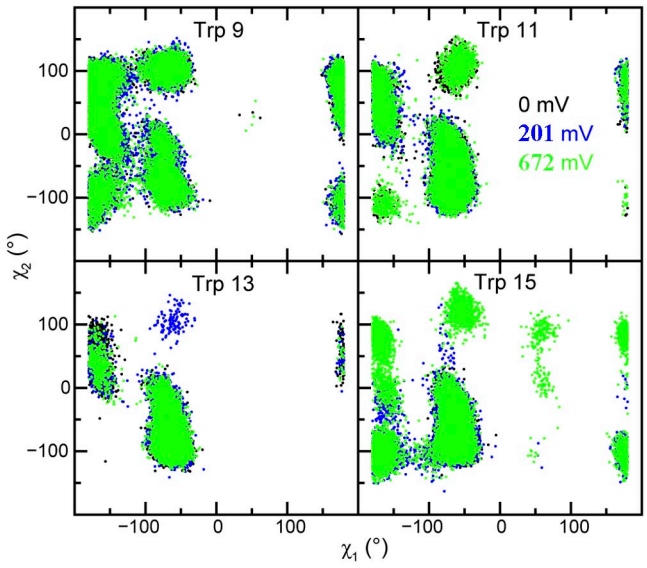

Figure S8. gA (1MAG) tryptophan (Trp) rotameric states at different applied voltages. These data indicate, in accordance with Fig. S7, that the average orientation of the Trp residues is independent of the applied field. Consequently, voltage-dependent reorientation of the Trp residues appears not to influence ion permeation. See the Fig. S4 legend for more details.

Table S1

$K_V1.2/2.1$ simulations

Simulation	t	E	$\langle l_z \rangle$	V	N_K	$N_{K,cav}$	I_K	$I_{K,cav}$	I_W	I_W/I_K	O	τ_{mwt}	τ_{res}/O	$\tau_{mwt} - \tau_{res}/O$
1	18	0.2000	86.8 ± 0.2	752.9 ± 1.4	4,196	8,162	21.12 ± 2.83	40.56 ± 73.71	14.40 ± 0.60	0.68 ± 0.10	2.54	0.8 ± 0.1	0.4 ± 0.0	0.4 ± 0.1
2	14	0.1750	86.5 ± 0.2	656.4 ± 1.2	1,472	1,463	16.47 ± 1.30	16.28 ± 1.19	9.40 ± 0.63	0.57 ± 0.06	2.68	1.0 ± 0.1	1.0 ± 0.0	0.0 ± 0.1
3	17	0.1500	86.4 ± 0.1	561.9 ± 0.9	1,373	1,403	13.37 ± 0.77	13.59 ± 0.73	6.74 ± 0.63	0.50 ± 0.06	2.67	1.2 ± 0.1	1.2 ± 0.0	0.0 ± 0.1
4	10	0.1375	86.6 ± 0.1	516.4 ± 0.5	599	647	9.67 ± 1.10	10.29 ± 1.11	3.97 ± 0.58	0.41 ± 0.08	2.87	1.7 ± 0.2	1.6 ± 0.0	0.1 ± 0.2
5	10	0.1250	86.9 ± 0.1	471.2 ± 0.5	375	515	6.05 ± 0.63	8.19 ± 0.47	3.25 ± 0.38	0.54 ± 0.08	2.78	2.7 ± 0.3	2.5 ± 0.1	0.1 ± 0.3
6	15	0.1250	86.9 ± 0.1	471.1 ± 0.6	567	764	5.91 ± 0.69	7.89 ± 0.50	3.15 ± 0.33	0.53 ± 0.08	2.76	2.7 ± 0.3	2.6 ± 0.1	0.1 ± 0.3
7	44	0.1000	86.7 ± 0.2	375.8 ± 0.8	358	604	4.16 ± 0.42	7.00 ± 0.32	1.63 ± 0.15	0.39 ± 0.05	2.90	3.8 ± 0.4	3.6 ± 0.1	0.3 ± 0.4
8	22	0.0750	86.6 ± 0.1	281.6 ± 0.4	152	386	1.77 ± 0.47	4.79 ± 0.88	0.76 ± 0.13	0.43 ± 0.14	2.45	9.2 ± 2.4	7.9 ± 0.6	1.2 ± 2.4
9	22	0.0500	87.1 ± 0.1	188.9 ± 0.2	60	520	0.44 ± 0.11	3.72 ± 0.32	0.48 ± 0.15	1.09 ± 0.44	2.44	36.3 ± 9.0	31.2 ± 3.5	5.1 ± 9.7
10	40	0.0250	87.6 ± 0.1	94.9 ± 0.1	11	575	0.05 ± 0.04	2.30 ± 0.18	0.55 ± 0.12	1.91 ± 0.97	2.08	310.4 ± 213.9	112.6 ± 30.9	197.8 ± 216.1
11	22	0.0125	87.3 ± 0.3	47.3 ± 0.1	20	331	0.17 ± 0.04	2.36 ± 0.64	0.16 ± 0.08	0.97 ± 0.52	2.33	96.7 ± 25.4	74.9 ± 8.9	21.8 ± 26.9
12[a]	29	0.1000	130.9 ± 0.2	567.5 ± 1.0	1,820	2,031	9.98 ± 0.63	10.69 ± 0.55	6.09 ± 0.70	0.61 ± 0.08	2.58	1.6 ± 0.1	1.6 ± 0.0	0.0 ± 0.1
13[b]	18	0.1000	152.4 ± 0.2	661.0 ± 1.0	1,847	1,784	16.41 ± 1.31	15.69 ± 1.49	27.39 ± 13.80	1.67 ± 0.85	2.44	1.0 ± 0.1	1.0 ± 0.0	0.0 ± 0.1
14[c]	16	0.060	144.7 ± 0.4	376.5 ± 1.0	237	568	2.58 ± 0.33	6.15 ± 0.52	—	—	—	—	—	—
15[c]	15	0.060	151.4 ± 0.1	393.9 ± 0.3	168	431	1.72 ± 0.51	4.55 ± 0.32	—	—	—	—	—	—
16[d]	23	0.1000	87.8 ± 0.1	380.6 ± 0.4	318	1,020	2.20 ± 0.17	6.99 ± 12.63	1.68 ± 0.24	0.76 ± 0.13	2.62	7.3 ± 0.6	7.2 ± 0.3	0.113 ± 0.6
17[d]	13	0.1000	130.8 ± 0.1	567.2 ± 0.8	531	604	6.53 ± 0.48	27.96 ± 3.64	4.40 ± 0.49	0.67 ± 0.09	2.51	2.5 ± 0.2	1.0 ± 0.0	1.432 ± 0.2
18[e,f]	6	0.1500	87.0 ± 0.2	565.9 ± 1.0	196	194	10.59 ± 2.6	—	8.22 ± 2.89	0.78 ± 0.33	0.23	1.5 ± 0.4	11.9 ± 1.1	−10.4 ± 1.2
19[f]	28	0.0500	87.0 ± 0.2	188.6 ± 0.4	28	119	0.34 ± 0.10	—	0.08 ± 0.03	0.23 ± 0.11	1.70	47.1 ± 13.8	30.0 ± 4.8	16.8 ± 14.6
20[f]	35	0.0250	87.4 ± 0.2	94.7 ± 0.2	9	33	0.18 ± 0.07	—	0.08 ± 0.02	0.44 ± 0.21	1.99	88.9 ± 34.6	133.0 ± 54.5	−44.1 ± 64.6
21[f]	18	0.0125	87.0 ± 0.2	47.2 ± 0.1	6	46	0.09 ± 0.04	—	0.07 ± 0.04	0.78 ± 0.56	1.45	177.8 ± 79.0	69.0 ± 41.8	108.8 ± 89.4
22[g]	9(4)	0.075	80.9 ± 0.3	263.0 ± 1.0	8	44	0.30 ± 0.09	—	—	—	—	—	—	—
23[g]	10	0.175	81.2 ± 0.2	616.0 ± 1.8	205	222	3.23 ± 0.81	—	—	—	—	—	—	—
24[g]	9(8)	0.075	81.3 ± 0.3	264.4 ± 0.9	18	120	0.47 ± 0.23	—	—	—	—	—	—	—
25[g]	12(6)	0.150	81.4 ± 0.3	529.4 ± 1.6	68	92	1.68 ± 0.39	—	—	—	—	—	—	—

Total simulated time (t, μs), applied field (E; kcal · mol^{-1} · Å^{-1} · e^{-1}), average box length ($\langle l_z \rangle$; Å), applied voltage ($V = E \cdot \langle l_z \rangle$), K^+ permeation events across pore and cavity (N_K, $N_{K,cav}$), K^+ pore and cavity currents and water currents (I_K, $I_{K,cav}$, I_W; pA), ion-to-water permeation ratio (I_W/I_K), K^+ kinetic occupancy (O), mean waiting time between pore permeation events (τ_{mwt}; 10^{-8} s), K^+ SF residence time in sites S0–S5 (τ_{res}/O; occupancy normalized, summed over all sites, 10^{-8} s; see Figs. 2, C and E, and S1), mean waiting time and residence time difference ($\tau_{mwt} - \tau_{res}/O$; 10^{-8} s). The time in parentheses is the simulated time used for analysis in the three simulations where the pore underwent half (simulations 22 and 25) or full (simulation 23) pore closure because of the absent VSDs.

[a]n = 158k atoms.

[b]n = 186k atoms.

[c]n = 230k atoms with T1 retained; simulation 15 used CHARMM27 lipid parameters.

[d][KCl] = 0.3 M.

[e]The SF deteriorated after 5 μs.

[f]With σ (K^+–O) = 3.2874 Å.

[g]Pore-only "controls" in a palmitoyl oleoyl phosphatidylethanolamine membrane, as used previously in our pore-only simulations, with the force field–corrected SF. Simulations 22 and 23 used CHARMM36 lipid parameters (Klauda et al., 2010), whereas simulations 24 and 25 used the CHARMM27 lipid parameters (MacKerell et al., 1998) we used previously for POPE (Jensen et al., 2010).

Table S2
gA simulations

Simulation	t	E	$\langle l_z \rangle$	V	σ (K^+–O)	N_K	I_K	O
1	77	0.06	68.8	183.7	3.0859	7	0.02 ± 0.01	1.00
2	45	0.1	68.8	306.3	3.0859	14	0.06 ± 0.02	1.00
3	29	0.15	68.8	459.4	3.0859	40	0.22 ± 0.05	1.00
4	28	0.2	68.9	613.5	3.0859	93	0.55 ± 0.09	1.00
5	11	0.27	69.0	829.1	3.0859	107	1.61 ± 0.37	1.00
6	21	0.2	72.6	645.8	2.9399	5	0.06 ± 0.01	1.00
7	30	0.2	72.6	645.8	3.0000	26	0.16 ± 0.04	1.07[a]
8	35	0.2	72.6	645.8	3.1000	88	0.41 ± 0.07	1.00
9	31	0.2	72.5	645.6	3.1500	80	0.41 ± 0.08	1.00
10	30	0.2	72.5	645.6	3.2000	49	0.25 ± 0.05	1.01
11	5	0.2	72.5	645.6	3.2874	0	0	1.00[b]
12[c]	11	0.2	72.6	645.8	3.0000, 3.2000	0	0	1.00
13[c]	5	0.2	72.6	645.8	3.0859, 3.2000	0	0	1.00
14[c]	16	0.2	72.5	645.6	3.2000, 3.0000	47	0.47 ± 0.08	1.01
15[c]	11	0.2	72.5	645.6	3.0859, 3.0000	57	0.85 ± 0.15	1.00
16[c]	44	0.1	72.4	322.1	3.0859, 3.0000	22	0.08 ± 0.03	1.00
17[a]	5	0	77.2	0	3.0859	—	—	—
18[a]	7	0.06	77.4	201.2	3.0859	—	—	—
19[a]	7	0.2	77.5	671.7	3.0859	—	—	—
20[d]	10	0.15	68.8	459.4	3.0859	12	0.21 ± 0.07	1.00
21[e]	20	0.2	75.1	670.0	3.0859	10	0.11 ± 0.03	1.01
22[e]	11	0.27	74.0	890.0	3.0859	30	0.44 ± 0.14	1.01
23[f]	5	0	86.6	0	3.0859	—	—	—
24[f]	7	0.06	86.5	225.0	3.0859	—	—	—
25[f]	7	0.2	85.7	742.0	3.0859	—	—	—

Total simulated time (t; μs), applied field (E; kcal · mol^{-1} · $Å^{-1}$ · e^{-1}), average box length ($\langle l_z \rangle$; Å), applied voltage calculated as $V = E \cdot \langle l_z \rangle$, LJ K^+–O interaction parameter (σ; Å), K^+ permeation events (N_K), current (I_K; pA), and kinetic occupancy (O) of the pore.
[a]With no ions in the system. 10% of the configurations with a K^+ populated pore had two ions in the pore.
[b]Only 87 occurrences were observed with the ion being inside the pore at $-15 < z < 15$ Å.
[c]Different σ values were used for vestibule and lumen.
[d]Used the 1JNO structure (Townsley et al., 2001).
[e]Using CHARMM27 lipid parameters.
[f]Using CHARMM27 lipid parameters and with no ions in the system.

Table S3
gA permeation kinetics

Simulation	V	N_K	$N_{K,vestibule}$	I_K	$I_{K,vestibule}$	$I_K/I_{K,vestibule}$	τ_{mwt}	τ_{res}/O	$\tau_{mwt}-\tau_{res}/O$
5	829.1	107	96	1.61 ± 0.37	1.43 ± 0.25	1.13 ± 0.11	0.99	0.95	0.04
4	613.5	93	123	0.55 ± 0.09	0.73 ± 0.07	0.75 ± 0.02	2.89	1.99	0.9
3	459.4	40	75	0.22 ± 0.05	0.42 ± 0.07	0.52 ± 0.02	7.21	3.12	4.1
2	306.3	14	132	0.06 ± 0.02	0.47 ± 0.10	0.13 ± 0.00	27.03	2.31	24.7
1	183.7	7	240	0.02 ± 0.01	0.50 ± 0.05	0.04 ± 0.00	90.11	0.54	89.6

Applied voltage (V; mV), K^+ permeation events across pore and vestibule (N_K, $N_{K,vestibule}$; a buffer region of 2 Å was used in vestibule calculations), pore and vestibule currents (I_K, $I_{K,vestibule}$; pA). The latter comprises current across minima 1 and 3 in Fig. 4 D in the main text, their ratio ($I_K/I_{K,vestibule}$), mean waiting time between permeation events (τ_{MWT}; 10^{-7} s), cumulative K^+ pore residence time (τ_{res}/O; summed over minima 1–10 in Fig. 4 D and occupancy normalized, $O = 1$; 10^{-7} s), and difference between mean waiting and residence times (entry time, $\tau_{mwt} - \tau_{res}/O$; 10^{-7} s).

Table S4

K^+ transition ratios in gA

Simulation	t	E	V	σ (K^+–O)	I_K (pA)	1→2	2→3	3→4	4→5	2→3/1→2	3→4/2→3	4→5/3→4
1	77	0.06	183.7	3.0859	0.02 ± 0.01	14,795	815	153	43	0.1	0.2	0.3
2	45	0.10	306.3	3.0859	0.06 ± 0.02	8,692	837	211	35	0.1	0.3	0.2
3	29	0.15	459.4	3.0859	0.22 ± 0.05	5,199	893	288	128	0.2	0.3	0.4
4	28	0.20	613.5	3.0859	0.55 ± 0.09	4,292	1,171	506	174	0.3	0.4	0.4
5	11	0.27	829.1	3.0859	1.61 ± 0.37	1,310	546	251	144	0.4	0.5	0.6
6	21	0.20	645.8	2.9399	0.06 ± 0.01	2,056	466	164	30	0.2	0.4	0.2
11	5	0.20	645.6	3.2874	0	165	3	0	1	0.0	0	—
12[a]	11	0.20	645.8	3.0000, 3.2000	0	3,429	11	0	0	0.0	0	—
13[a]	5	0.20	645.8	3.0859, 3.2000	0	997	96	10	2	0.1	0.1	0.2
14[a]	16	0.20	645.6	3.2000, 3.0000	0.47 ± 0.08	1,376	79	31	48	0.1	0.4	1.6
15[a]	11	0.20	645.6	3.0859, 3.0000	0.85 ± 0.15	1,564	363	425	184	0.2	1.1	0.4
16[a]	44	0.10	322.1	3.0859, 3.0000	0.08 ± 0.03	8,213	1,150	650	171	0.1	0.6	0.3

Total simulated time (t; μs), applied field (E; kcal · mol^{-1} · $Å^{-1}$ · e^{-1}), applied voltage (V; mV), LJ K^+–O interaction parameter (σ; Å), and current (I_K; pA). For an idealized linear *I-V* curve, the individual transition ratios would remain constant across all voltages, whereas the absolute number of transitions would be proportional to the magnitude of voltage. The percentage of K^+ transitions from site 2 to site 3 relative to transitions from site 1 to 2—the 2→3/1→2 ratio (see Fig. 4 D in the main text)—differs about fourfold between lowest and highest voltages. In contrast, corresponding variation of the 4→5/3→4 ratio is only about twofold.

[a]Dual σ values were used for vestibule and lumen.

Table S5

KcsA simulations with native and weakened SF–K^+ interactions

Simulation	t	E	$\langle l_z \rangle$	V	N_K	I_K	I_W	I_W/I_K	O
Native	2	0.10	96.3	428.5	257	25.59 ± 2.43	0.73 ± 0.42	0.03 ± 0.02	3.25
Weakened	2	0.10	96.1	427.4	19	1.63 ± 0.44	0.77 ± 0.36	0.47 ± 0.26	2.16
Asp80 "up"	2	0.10	96.1	427.5	188	19.11 ± 1.91	0	0	2.83
Ala71Glu	2	0.15	95.6	638.1	200	21.74 ± 3.53	9.64 ± 1.48	0.44 ± 0.10	2.91
Asp80Asn	2	0.15	95.0	634.1	168	15.65 ± 6.51	3.52 ± 1.64	0.23 ± 0.14	3.33

The Asp80 χ_1 side chain was in one simulation restrained to pointing into the extracellular solution ("up," as the corresponding residue is predominantly oriented in $K_V1.2/2.1$) using dihedral restraints with a force constant of 9 kcal · mol^{-1} · rad^{-2}. Two simulations, one with Glutamate at position 71 ("Ala71Glu") and one with an Asp80Asn mutant ("Asp80Asn") were carried out to examine the effects of introducing protonated Glu in the SF region and of removing the Asp80 negative charge, respectively. For each simulation the following are listed: the total simulated time (t; μs), applied field (E; kcal · mol^{-1} · $Å^{-1}$ · e^{-1}), average box length ($\langle l_z \rangle$; Å), applied voltage calculated as $V = E \cdot \langle l_z \rangle$, K^+ permeation events (N_K), K^+ and water currents (I_K, I_W; pA), ion-to-water permeation ratio (I_W/I_K), and K^+ kinetic occupancy (O).